

pubs.acs.org/NanoLett Letter

# Electrically Switchable Intervalley Excitons with Strong Two-Phonon Scattering in Bilayer WSe<sub>2</sub>

Mashael M. Altaiary, ◆ Erfu Liu, ◆ Ching-Tarng Liang, Fu-Chen Hsiao, Jeremiah van Baren, Takashi Taniguchi, Kenji Watanabe, Nathaniel M. Gabor, Yia-Chung Chang,\* and Chun Hung Lui\*



Cite This: Nano Lett. 2022, 22, 1829–1835



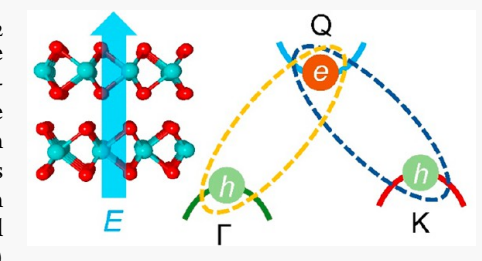
**ACCESS** 

Metrics & More

Article Recommendations

s Supporting Information

**ABSTRACT:** We report the observation of  $Q\Gamma$  intervalley exciton in bilayer WSe<sub>2</sub> devices encapsulated by boron nitride. The  $Q\Gamma$  exciton resides at ~18 meV below the QK exciton. The  $Q\Gamma$  and QK excitons exhibit different Stark shifts under an out-of-plane electric field due to their different interlayer dipole moments. By controlling the electric field, we can switch their energy ordering and control which exciton dominates the luminescence of bilayer WSe<sub>2</sub>. Remarkably, both  $Q\Gamma$  and QK excitons exhibit unusually strong two-phonon replicas, which are comparable to or even stronger than the one-phonon replicas. By detailed theoretical simulation, we reveal the existence of numerous ( $\geq$ 14) two-phonon scattering paths involving (nearly)



resonant exciton—phonon scattering in bilayer WSe<sub>2</sub>. To our knowledge, such electric-field-switchable intervalley excitons with strong two-phonon replicas have not been found in any other two-dimensional semiconductors. These make bilayer WSe<sub>2</sub> a distinctive valleytronic material with potential novel applications.

**KEYWORDS:** bilayer WSe<sub>2</sub>, QK intervalley exciton,  $Q\Gamma$  intervalley exciton, Stark shift, phonon replicas, two-phonon scattering

hen a system hosts multiple competing states, intriguing and complex physics can emerge. Prominent examples include the competing optical modes in a laser, bistable modes in electronics and optics, and competing spin orders in magnetic materials; the properties of these systems can be switched sensitively by the external conditions. For semiconductors, if a material hosts two tunable and competing low-lying states, then their interplay can produce intricate optical spectra and enable versatile material engineering. For instance, one may tune the luminescent spectrum of the material by switching the energy ordering of the states. Also, resonant phonon scattering may occur between two nearly degenerate states, leading to strong electron—phonon coupling. As a result, the material can exhibit a highly tunable spectrum with possibly strong phonon-assisted emission.

2H-stacked bilayer WSe<sub>2</sub> (Figure 1a,b) is a distinctive material to realize such a novel tunable electron—phonon system. First, it hosts two competing low-lying excitons, namely, the QK and QΓ intervalley excitons ( $X_{\rm QK}$ ,  $X_{\rm QΓ}$ ), which are associated with one Γ valence valley at the zone center, two K valence valleys (K, K') at the zone corners, and six Q conduction valleys (Q, Q') in the Brillouin zone (Figure 1c,d). Although the electronic structure suggests the QK exciton as the lowest-lying exciton, recent theoretical research shows that the QΓ exciton may have similar energy due to the large effective mass of the Γ valley. Such competing intervalley excitons can hardly be found in other transition metal dichalcogenides (TMDs), such as MoS<sub>2</sub>, MoSe<sub>2</sub>, and WS<sub>2</sub>. Second, the QK and QΓ exciton energies can be

significantly tuned by electric field. As the QK and Q $\Gamma$  excitons possess different interlayer electric dipole, by applying an out-of-plane electric field, we can adjust their energy separation through the Stark effect<sup>6,13,16–24</sup> (Figure 1e). Such field-tunability of excitons can hardly be realized in monolayer semiconductors. Third, WSe<sub>2</sub> is known to exhibit strong exciton—phonon interactions, signified by the pronounced phonon replicas in the optical spectra. <sup>15,25–30</sup> The above three distinctive characteristics constitute bilayer WSe<sub>2</sub> as a distinctive tunable exciton—phonon system with potential valleytronic applications. <sup>19,31–37</sup>

Experimental research of bilayer WSe $_2$  has, however, been much hindered by poor sample quality and its broad and weak optical spectra. For instance, although prior research has shown some theoretical and experimental evidence of QF exciton (e.g., in quantum-dot emission), 12 direct observation of the QF exciton in pristine bilayer TMDs has never been reported. Prior research also studied the Stark effect of QK excitons, 6,13,16–23 but the related studies of the QF Stark effect and the QK and QF phonon replicas are still lacking.

In this Article, by using ultraclean bilayer WSe<sub>2</sub> devices encapsulated by boron nitride (BN), we directly resolve the

Received: April 22, 2021 Revised: January 19, 2022 Published: February 24, 2022





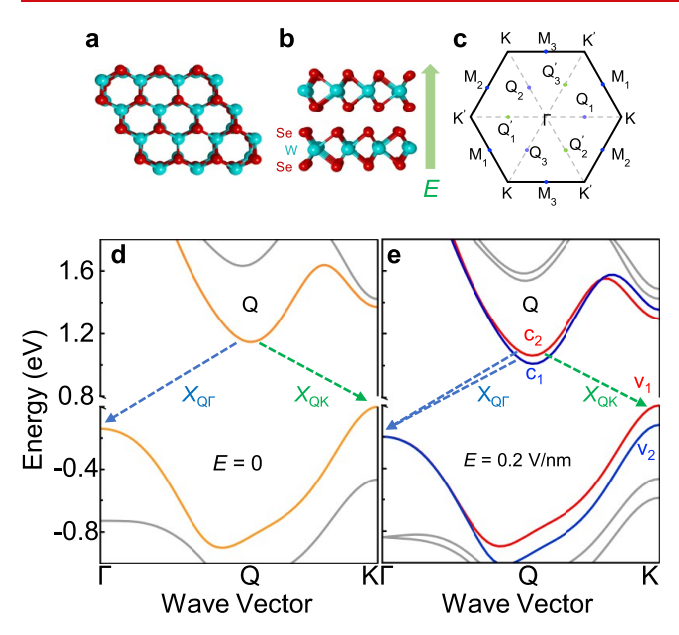


**Figure 1.** Electronic band structure of bilayer WSe<sub>2</sub>. (a) Top view and (b) side view of the crystal structure of 2H-stacked bilayer WSe<sub>2</sub>. (c) First Brillouin zone of bilayer WSe<sub>2</sub>. (d, e) Calculated electronic band structure along the K-Γ line at zero (d) and 0.2 V/nm (e) vertical electric field. Each band is doubly degenerate at zero field, but split at finite field (except at the Γ point). We denote the  $X_{\rm Q\Gamma}$  and  $X_{\rm QK}$  emission and the dominant spin-up (spin-down) polarization by red (blue) color. The Q and Q' states are energy-degenerate with opposite spins due to the time-reversal symmetry.

QΓ exciton emission and conduct comparative electric-fielddependent studies between the Q $\Gamma$  and QK excitons and phonon replicas. Contrary to the suggestion of the free-particle band structure (Figure 1d), we observe that the Q $\Gamma$  exciton lies at ~18 meV below the QK exciton; this reveals considerably stronger binding of the  $Q\Gamma$  exciton than the QK exciton. We also observe strong Stark effect in both excitons under an out-of-plane electric field, but the Q $\Gamma$  Stark shift is considerably weaker than the QK shift. By tuning the electric field strength between 0 and 0.11 V/nm, we can switch the energy order of the Q $\Gamma$  and QK excitons and control which exciton dominates the optical emission. Notably, both excitons exhibit strong two-phonon replicas, which are comparable to or even brighter than the one-phonon replicas and outshine the primary emission. We can simulate the replica spectra by comprehensive theoretical calculation. Our results reveal the existence of numerous two-phonon scattering processes with (nearly) resonant exciton-phonon scattering, which lead to unusually strong two-phonon replicas in bilayer WSe2. Overall, our research demonstrates bilayer WSe2 as a unique valleytronics material with switchable intervalley excitons and strong two-phonon scattering, which can hardly be found in other atomically thin semiconductors.

In our experiment, we fabricate dual-gate bilayer WSe<sub>2</sub> devices encapsulated by hexagonal boron nitride on Si/SiO<sub>2</sub> substrates (Figure 2a). The BN encapsulation significantly improves the sample quality and allows for the observation of Q $\Gamma$  exciton. Thin graphite flakes are used as the contact and gate electrodes to further enhance the device performance. By applying voltages of opposite signs and appropriate ratio on the top gate ( $V_{\rm tg}$ ) and bottom gate ( $V_{\rm bg}$ ), we can generate a vertical electric field across bilayer WSe<sub>2</sub> while keeping the sample charge neutral. The  $V_{\rm tg}$ : $V_{\rm bg}$  ratio depends on the gating-

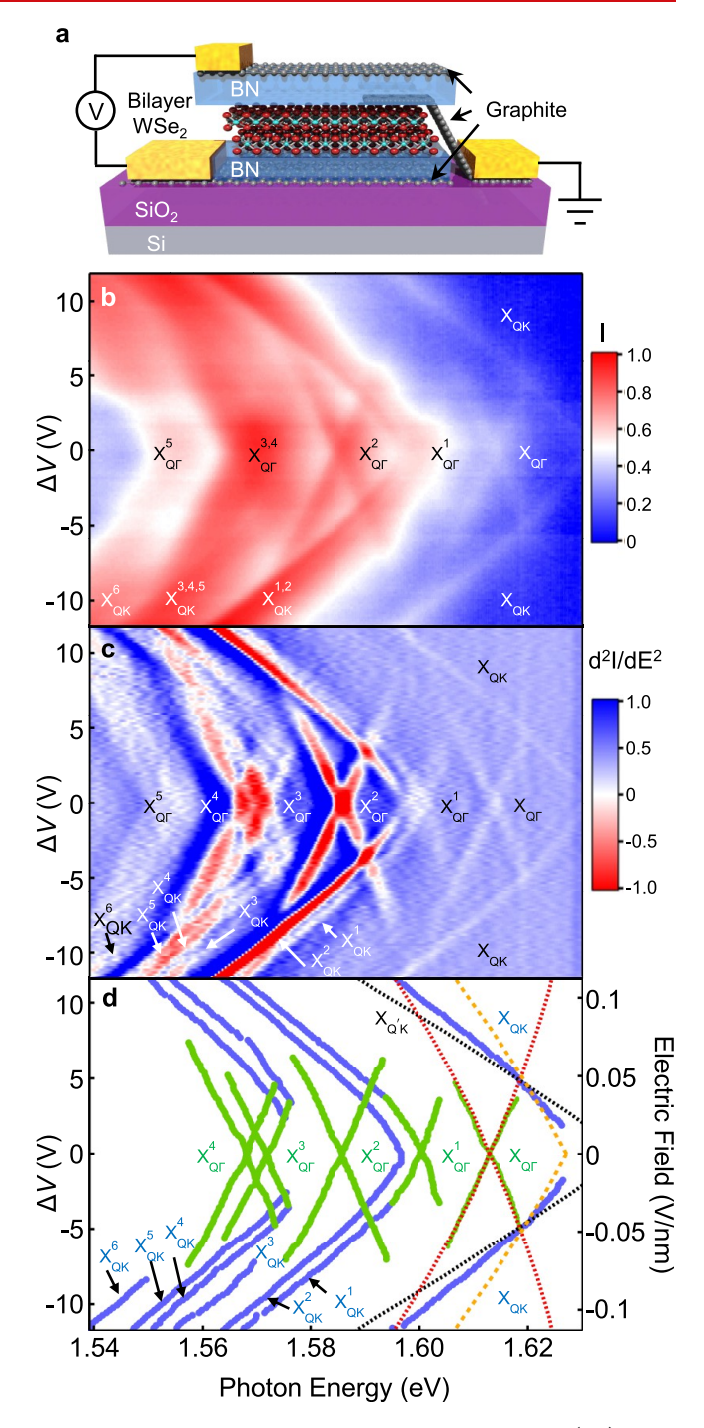


Figure 2. Electric-field-dependent photoluminescence (PL) of a bilayer WSe<sub>2</sub> device. (a) Schematic of our dual-gate BN-encapsulated bilayer WSe<sub>2</sub> devices. (b) PL map of a bilayer WSe<sub>2</sub> device at varying voltage difference  $\Delta V = V_{\rm tg} - V_{\rm bg}$  between the top and bottom gates while keeping the sample charge neutral. The measurements were conducted at temperature  $T \sim 15$  K under 730 nm continuous-wave laser excitation with incident power  $\sim 15~\mu W$ . (c) Second-order energy derivative of panel b. (d) Extracted energies of emission features in panel c. The primary QF and QK exciton emission ( $X_{\rm QF}$ ,  $X_{\rm QK}$ ) and phonon replicas ( $X_{\rm QF}^{1-5}$ ,  $X_{\rm QK}^{1-6}$ ) are denoted. The dashed lines are the calculated Stark shifts of the QF (red), QK (orange), and Q'K (black) spin-allowed optical transitions.

efficiency ratio of the top and bottom gates, which is affected by their different BN thickness, interfacial and dielectric Nano Letters pubs.acs.org/NanoLett Lette

environment. (See the Supporting Information for details of device fabrication and experiment.)

Figure 2b displays the photoluminescence (PL) map at varying voltage difference ( $\Delta V = V_{\rm tg} - V_{\rm bg}$ ) between the top and bottom gates at temperature  $T \sim 15$  K. At low  $\Delta V$ , we observe multiple X-shape emission features; such field-dependent X-shape features have never been reported in bilayer WSe<sub>2</sub>. At large  $\Delta V$ , several red-shifting lines appear; they should be associated with the QK exciton according to prior research.<sup>13</sup> We further worked out the second-order energy derivative on the PL map to resolve the fine features (Figure 2c). From the map of the second-order derivative, we extract the energies of different emission features and plot them as a function of electric field in Figure 2d.

We first consider the two sets of highest-energy features, which consist of one X-shape feature and two red-shifting lines in 1.60-1.63 eV (Figure 2b-d). They are significantly weaker than the replica features at lower energy. We tentatively assign them as the primary  $X_{\rm Q\Gamma}$  and  $X_{\rm QK}$  emission assisted by defect scattering (here "Q" includes all six Q and Q' valleys). Defect scattering is considered because direct optical recombination of intervalley excitons is forbidden by the momentum conservation. 27,28 To confirm our assignment, we conducted first-principles calculations on the band structure of bilayer WSe<sub>2</sub> under different vertical electric fields (Figure 1d,e). At zero field, each band is doubly degenerate due to the inversion and time-reversal symmetry of 2H-stacked bilayer WSe<sub>2</sub><sup>6,7,9</sup> (Figure 1d). At the finite electric field, the inversion symmetry is broken, and each band is split into two bands with opposite spins and layer polarizations (except at the  $\Gamma$  point due to the time-reversal symmetry) (Figure 1e). Consequently, the  $X_{Q\Gamma}$ and  $X_{\rm QK}$  emission lines are split and exhibit Stark shifts. We have calculated the energies of spin-allowed QΓ, QK, and Q'K optical transitions at different electric fields via density functional theory (DFT) (see the Supporting Information). The spin-allowed QK and Q'K transitions involve the upper and lower split conduction bands, respectively, because the Q and Q' states have opposite spins from each other; hence they have somewhat different Stark shifts. We neglect the influence of excitonic effect on the Stark shift, offset each theoretical transition energy to match the corresponding experimental energy, and focus our comparison only on the Stark shifts. The theoretical Stark shifts (dashed lines in Figure 2d) agree decently with our data and hence support the assignment of  $Q\Gamma$  and QK excitons.

The  $Q\Gamma$  exciton exhibits two remarkable characteristics. First,  $X_{\rm Q\Gamma}$  is ~18 meV lower than  $X_{\rm QK}$  and is significantly brighter than  $X_{\rm QK}$ . This result is surprising because the  $\Gamma$ valence valley is  $\sim$ 140 meV lower than the K valence valley in the electronic band structure (Figure 1d);  $^{11,38-40}$  one would naturally expect that the  $Q\Gamma$  transition has higher energy than the QK transition. However, further examination of the band structure reveals that the  $\Gamma$  valley has a much larger hole effective mass ( $\sim$ 1.48 $m_0$ ;  $m_0$  is the free electron mass) than the K valence valley  $(\sim 0.43 m_0)^{40}$  (Table S1). The Q $\Gamma$  exciton also has stronger intervalley mixing effect than the QK exciton. Th larger effective mass and stronger intervalley mixing effect make the  $Q\Gamma$  exciton bind more strongly than the QK exciton (see Supporting Information, Section 7.2). The larger exciton binding energy causes  $X_{\text{OF}}$  to have lower energy than  $X_{\text{OK}}$ . This result is significant because the lowest excitonic state plays a paramount role in the excitonic dynamics and luminescence.

Second, the  $X_{\rm Q\Gamma}$  Stark shift (~135 meV per 1 V/nm field) is 1.9 ~ 2.7 times weaker than the  $X_{\rm QK}$  Stark shift (265 ~ 360 meV per 1 V/nm field). This can be qualitatively understood from their different charge density distribution. Figure 3 shows

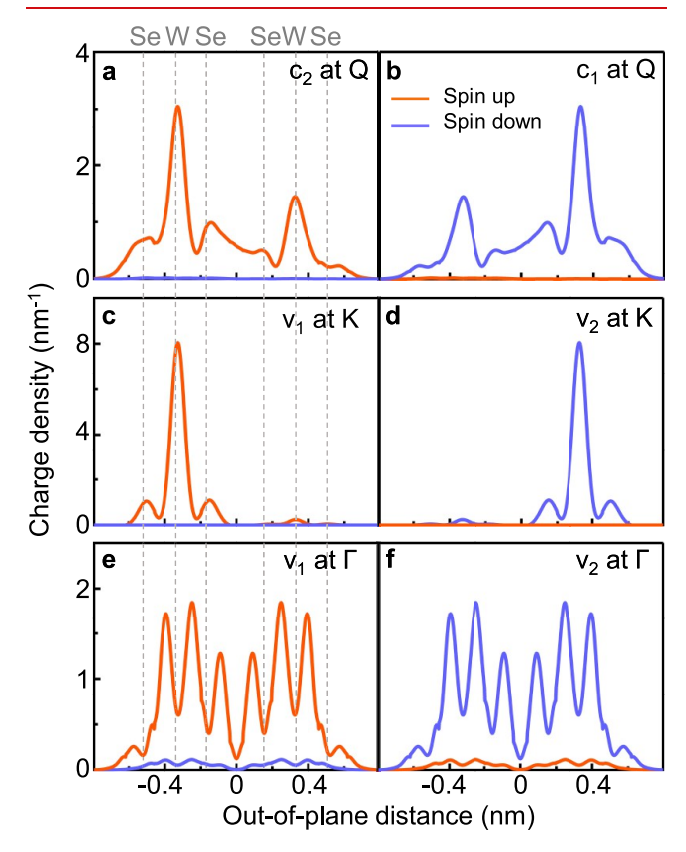


Figure 3. Calculated spin-dependent in-plane-averaged charge density along the out-of-plane direction. (a, b) Density for the electron states at the Q point of the conduction bands  $c_1$  and  $c_2$ . The time-reversal states at the Q' point have the same density distribution but opposite spin. (c–f) Density for the states at the K and  $\Gamma$  points of the valence bands  $v_1$  and  $v_2$ . An infinitesimal vertical electric field is considered to separate the states. The states at  $c_1$   $(v_1)$  and  $c_2$   $(v_2)$  have opposite spin and layer polarization. The vertical dashed lines denote the central position of the atoms. We note that the density maxima of the  $\Gamma$ -point electrons are not at the center of the atoms due to their specific orbitals.

our calculated spin-dependent charge density along the vertical direction for electron states at the Q, K, and  $\Gamma$  points (the Q' states have the same density distribution as the Q states but opposite spin). We consider an infinitesimal electric field to break the inversion symmetry. The separated states show strong spin polarization; the electric field essentially splits them into spin-up and spin-down states. The K, Q, and  $\Gamma$  states show different layer polarization. The Q conduction states show medium layer polarization with an electric dipole moment  $p_Q = 0.107$  e·nm, where  $e = 1.6 \times 10^{-19}$  C is the elementary electric charge (Figure 3a, b). In contrast, the K valence states are strongly localized in opposite layers, giving rise to a large dipole moment  $p_{\rm K} = 0.307~e \cdot {\rm nm}$  (Figure 3c, d). At the other extreme, the two  $\Gamma$  valence states show symmetric distribution on the two layers, which produces no layer polarization and zero electric dipole moment ( $p_{\Gamma} = 0$ ) (Figure 3e,f). By combining these dipole moments, we estimate that a Q $\Gamma$  electron—hole pair has a dipole moment of  $p_{Q\Gamma} = p_Q - p_{\Gamma}$ 

Nano Letters pubs.acs.org/NanoLett Letter

= 0.107 *e*·nm, and an optically active QK (Q'K) electron—hole pair has a dipole moment of  $p_{\rm QK}=p_{\rm K}-p_{\rm Q}=0.200~e$ ·nm ( $p_{\rm Q'K}=p_{\rm K}+p_{\rm Q}=0.417~e$ ·nm). The average of  $p_{\rm QK}$  and  $p_{\rm Q'K}$  ( $\sim$ 0.3 *e*·nm) is about three times of  $p_{\rm Q\Gamma}$ . This roughly accounts for the difference between the  $X_{\rm Q\Gamma}$  and  $X_{\rm QK}$  Stark shift.

The different Stark shifts between  $X_{\rm Q\Gamma}$  and  $X_{\rm QK}$  have an interesting consequence—they allow us to use the electric field to switch the energy order and dominant luminescence between  $X_{\rm Q\Gamma}$  and  $X_{\rm QK}$  (Figures 2b and S6). When the electric field is weak (e.g.,  $E < 0.02 \ {\rm V/nm}$ ),  $X_{\rm Q\Gamma}$  lies well below  $X_{\rm QK}$  and dominates the emission due to its higher population. As the field increases,  $X_{\rm QK}$  gradually redshifts to become lower in energy than  $X_{\rm Q\Gamma}$ , and the exciton population transfers from  $X_{\rm Q\Gamma}$  to  $X_{\rm QK}$ ; this brightens  $X_{\rm QK}$  and suppresses  $X_{\rm Q\Gamma}$ . At strong electric field (e.g.,  $E > 0.08 \ {\rm V/nm}$ ),  $X_{\rm QK}$  dominates the luminescence. Such electric-field-switchable excitons are not found in monolayer TMDs and may find novel applications for bilayer WSe<sub>2</sub>.

After we address the primary  $X_{\rm Q\Gamma}$  and  $X_{\rm QK}$  emission, we turn to their replica emission at lower energy. Figure 2 shows five  $X_{\rm Q\Gamma}$  replicas  $(X_{\rm Q\Gamma}^1-X_{\rm Q\Gamma}^5)$  with respective redshift energies 13.0, 27.6, 41.7, 45.7, and 57.7 meV from  $X_{\rm Q\Gamma}$  and six  $X_{\rm QK}$  replicas  $(X_{\rm QK}^1-X_{\rm QK}^6)$  with respective redshift energies 28.8, 32.4, 41.9, 46.2, 49.1, and 58.3 meV from  $X_{\rm QK}$  (the uncertainty of these energies is from  $\pm 1$  to  $\pm 2$  meV; Table S6). The replicas exhibit identical Stark shifts to the primary emission lines. We tentatively attribute them to excitonic luminescence assisted by phonon emission, as phonon replicas have been reported in monolayer WSe<sub>2</sub>. Separately brighter than the primary emission, indicating that phonon-assisted emission is more efficient than defect-assisted emission in our system.

To identify the phonon replicas, we have calculated the phonon band structure of bilayer WSe2 with a rigid-ion model (Figure S11). Afterward, we calculate the one-phonon replicas for  $X_{O\Gamma}$  and  $X_{OK}$  by the perturbation theory. All of these calculations are done with zero external electric field. In our theory, the initial excitonic state is scattered to a second excitonic state by emitting a phonon, and the second state decays to emit a photon. The second state is not necessarily a bound exciton, but it must be a momentum-direct exciton in order to emit the photon. Momentum conservation restricts the one-phonon scattering processes to occur only through two paths. For  $X_{O\Gamma}$ , the electron may be scattered from Q to  $\Gamma$  by emitting a phonon  $(X_{\mathrm{Q}\Gamma} \to X_{\Gamma\Gamma})$ , or the hole may be scattered from  $\Gamma$  to Q by emitting a phonon  $(X_{Q\Gamma} \to X_{QQ})$ . Similarly, for  $X_{\rm QK}$ , the electron can be scattered from Q to K ( $X_{\rm QK} \to X_{\rm KK}$ ), or the hole can be scattered from K to  $Q(X_{OK} \rightarrow X_{OO})$ . As the initial  $X_{O\Gamma}$  and  $X_{OK}$  excitons can be associated with any of the six Q valleys and two K valleys, the momentum of the emitted phonons will be near one of the six Q points for  $X_{O\Gamma}$  and near one of the Q or M points for  $X_{OK}$ . The emitted phonon can come from any phonon branch, so the one-phonon replica spectra can exhibit multiple peaks (see Table S3 and Figure S12). These one-phonon scattering processes are all nonresonant, so the one-phonon replicas are generally weak.

Figure 4 compares our calculated one-phonon spectra for  $X_{\rm Q\Gamma}$  and  $X_{\rm QK}$  with the experimental spectra. We phenomenologically broaden the theoretical spectra by 2 meV to match the experimental peak width. The theoretical one-phonon spectra can account for the  $X_{\rm Q\Gamma}^{-1}$  peak, which is contributed dominantly by the LA and TA acoustic phonons near the Q points. It can also partially explain  $X_{\rm Q\Gamma}^{-2}$  and  $X_{\rm OK}^{-1,2}$ . But other

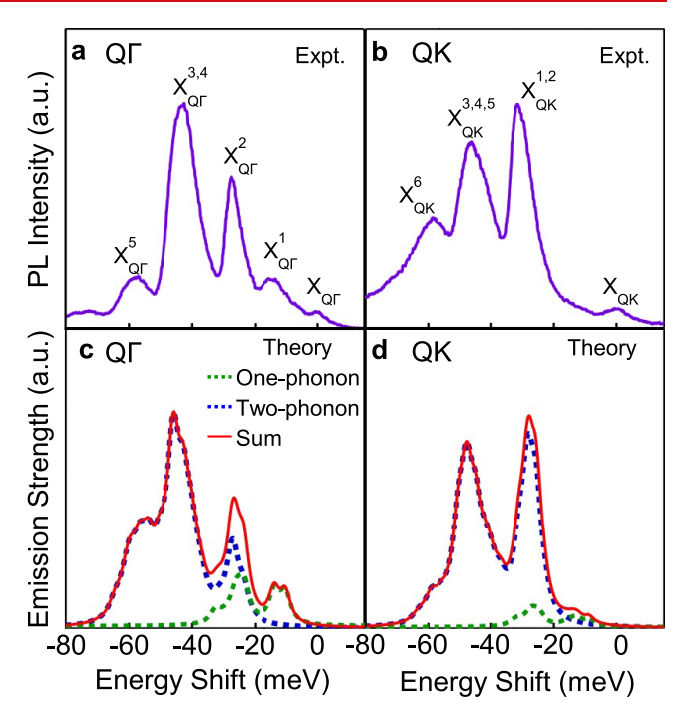


Figure 4. Theoretical simulation of the phonon-replica spectra. (a) Experimental Q $\Gamma$  emission spectrum at  $\Delta V=0$  in Figure 2b, offset by the  $X_{Q\Gamma}$  energy. (b) Experimental QK emission spectrum at  $\Delta V=-10~\rm V$  in Figure 2b, offset by the  $X_{\rm QK}$  energy. (c, d) Simulated spectra of one- and two-phonon replicas for  $X_{\rm Q\Gamma}$  (c) and  $X_{\rm QK}$  (d). Both theoretical spectra are broadened for 2 meV to match the experimental peak widths.

replicas  $(X_{\rm Q\Gamma}^{3-5})$  and  $X_{\rm QK}^{3-6}$  exceed the range of single-phonon energy (~37 meV) in WSe<sub>2</sub>. We would need to consider higher-order scattering processes to explain these replicas.

We have conducted comprehensive calculations on the twophonon replicas of  $X_{Q\Gamma}$  and  $X_{QK}$  with zero external electric field (see the Supporting Information for details). In our theory, the initial exciton is scattered to a second excitonic state by emitting a phonon and afterward scattered to a third excitonic state by emitting another phonon, and the third state decays to emit a photon. The second and third states are not necessarily bound excitons, but the third state may be a momentum-direct exciton in order to emit the photon. In contrast to the one-phonon processes with only two scattering paths, the two-phonon processes have numerous scattering paths. In our calculation, we only consider those scattering paths involving a resonant or nearly resonant exciton—phonon scattering process. In bilayer WSe2, the six Q conduction valleys are energy-degenerate, and  $X_{\mathrm{Q}\Gamma}$  and  $X_{\mathrm{Q}\mathrm{K}}$  are close in energy (~18 meV). Thus, carrier-phonon scattering between different Q valleys, between the  $\Gamma$  and K valence valleys, or within the same valley, is resonant or nearly resonant. Twophonon processes involving such (nearly) resonant scattering are expected to contribute dominantly to the replica spectra.

In our survey, there are totally 16 two-phonon scattering paths with a (nearly) resonant component for Q $\Gamma$  exciton. They can be separated into four groups:  $X_{\rm Q}\Gamma \to X_{\rm Q'}\Gamma \to X_{\rm Q'}\Gamma$ ;  $X_{\rm Q}\Gamma \to X_{\rm Q}\Gamma \to X_{$ 

Nano Letters pubs.acs.org/NanoLett Letter

Information for the explanation of these paths). Momentum conservation restricts the emitted phonons to be near the  $\Gamma$ , K, Q, and M points. As the emitted phonons can come from any phonon branch, the two-phonon replica spectra are rather complicated (see Tables S3 and S5 and Figure S13).

Figure 4c,d displays our calculated and broadened two-phonon replica spectra, which include contributions from all the above-mentioned scattering paths and all phonon branches. By summing the one-phonon and two-phonon spectra, our total theoretical spectra decently match the experimental spectra, including the energy and relative intensity of different replica peaks. From the theoretical results, we can attribute  $X_{\rm Q\Gamma}^{-1}$  to the one-phonon replica of Q-point acoustic phonons,  $X_{\rm Q\Gamma}^{-2}$  to a superposition of one-phonon and two-phonon replicas, and  $X_{\rm Q\Gamma}^{2-5}$  and  $X_{\rm QK}^{-1-6}$  to two-phonon replicas (see Table S6 for detailed assignments of each replica peak). In particular,  $X_{\rm QK}^{-1-5}$  are dominantly contributed by two-phonon paths involving the  $X_{\rm QK} \to X_{\rm Q\Gamma}$  transition with acoustic phonon emission, because this transition is strongly resonant when the emitted phonon energy is close to the 18-meV difference between  $X_{\rm QK}$  and  $X_{\rm Q\Gamma}$  (Table S5).

We remark that the two-phonon replicas are considerably stronger than the one-phonon replicas. This characteristic is counterintuitive because second-order processes are usually much weaker than first-order processes. There are two reasons for this unusual phenomenon. First, one of the scattering components in the two-phonon processes is (nearly) resonant. This makes each considered two-phonon process as strong as a nonresonant one-phonon process. Second, the number of (nearly) resonant two-phonon scattering paths ( $\geq$ 14) significantly exceeds the number of one-phonon scattering paths (only 2). After summing the contributions of these two-phonon paths, the total two-phonon spectra become considerably stronger than the one-phonon spectra.

We also note that the numerous resonant scattering channels are related to the existence of six degenerate Q valleys and two degenerate K valleys in bilayer  $WSe_2$  and are hence rare in condensed matter systems. They are not found in monolayer  $WSe_2$  or other TMDs due to the large energy separation between the QK and Q $\Gamma$  excitons in these systems. Therefore, bilayer  $WSe_2$  is a quite distinctive system to study novel exciton—phonon phenomena.

In sum, we have observed electric-field-switchable Q $\Gamma$  and QK intervalley excitons with unusually strong two-phonon replicas in bilayer WSe<sub>2</sub>. In the Supporting Information, we also show the Zeeman splitting effect of  $X_{\rm Q}\Gamma^2$  under magnetic field, from which we deduce a g-factor of  $9.1\pm0.4$  for the Q $\Gamma$  exciton<sup>12</sup> (Figure S3). The interesting interplay between excitons, phonons, and electric and magnetic fields, as demonstrated in our research, makes bilayer WSe<sub>2</sub> a distinctive exciton—phonon system with potential applications in excitonics and valleytronics.

After we submitted our manuscript, we became aware of a related work by another research team. 41

### ASSOCIATED CONTENT

# **Solution** Supporting Information

The Supporting Information is available free of charge at https://pubs.acs.org/doi/10.1021/acs.nanolett.1c01590.

Details on the device fabrication, experimental methods, determination of the electric field, Zeeman splitting of

the  $Q\Gamma$  exciton emission, results of another bilayer  $WSe_2$  device, and theoretical calculations (PDF)

# AUTHOR INFORMATION

#### **Corresponding Authors**

Yia-Chung Chang — Research Center for Applied Sciences, Academia Sinica, Taipei 11529, Taiwan; ⊚ orcid.org/0000-0003-1851-4651; Email: yiachang@gate.sinica.edu.tw

Chun Hung Lui — Department of Physics and Astronomy, University of California, Riverside, California 92521, United States; Email: joshua.lui@ucr.edu

#### **Authors**

Mashael M. Altaiary — Department of Physics and Astronomy, University of California, Riverside, California 92521, United States; Department of Physics, University of Jeddah, Jeddah 23445, Saudi Arabia

Erfu Liu — Department of Physics and Astronomy, University of California, Riverside, California 92521, United States;
orcid.org/0000-0002-0231-798X

Ching-Tarng Liang — Research Center for Applied Sciences, Academia Sinica, Taipei 11529, Taiwan

Fu-Chen Hsiao — Research Center for Applied Sciences, Academia Sinica, Taipei 11529, Taiwan; Advanced Semiconductor Device and Integration Laboratory, Department of Electrical and Computer Engineering, University of Illinois at Urbana—Champaign, Urbana, Illinois 61801, United States

Jeremiah van Baren – Department of Physics and Astronomy, University of California, Riverside, California 92521, United States

Takashi Taniguchi — International Center for Materials Nanoarchitectonics (WPI-MANA), National Institute for Materials Science, Ibaraki 305-0044, Japan; orcid.org/0000-0002-1467-3105

Kenji Watanabe — Research Center for Functional Materials, National Institute for Materials Science, Tsukuba 305-0044, Japan; © orcid.org/0000-0003-3701-8119

Nathaniel M. Gabor – Department of Physics and Astronomy, University of California, Riverside, California 92521, United States; Canadian Institute for Advanced Research, Toronto, Ontario MSG 1M1, Canada

Complete contact information is available at: https://pubs.acs.org/10.1021/acs.nanolett.1c01590

# **Author Contributions**

◆M.M.A. and E.L. contributed equally to this work.

#### Notes

The authors declare no competing financial interest.

# ACKNOWLEDGMENTS

We thank Fatemeh Barati and Matthew Wilson for help in the project, Ao Shi for assistance in manuscript preparation, Kin Fai Mak and Jie Shan for discussion, Yong-Tao Cui for supporting E.L., Harry Tom for equipment support, and Zhengguang Lu, Dmitry Smirnov, and Stephen McGill for assistance in magneto-optical experiments. C.H.L. acknowledges support from the National Science Foundation Division of Materials Research CAREER Award No. 1945660 and the American Chemical Society Petroleum Research Fund No. 61640-ND6. Y.-C.C. acknowledges support by the Ministry of Science and Technology (Taiwan) under Grant No. MOST

109-2112-M-001-046. N.M.G acknowledges support from the National Science Foundation Division of Materials Research CAREER Award No. 1651247, from the United States Department of the Navy Historically Black Colleges, Universities, and Minority Serving Institutions (HBCU/MI) Award No. N00014-19-1-2574, and from the Army Research Office Electronic Division Award No.W911NF2110260. K.W. and T.T. acknowledge support from the Elemental Strategy Initiative conducted by the MEXT, Japan and the CREST (JPMJCR15F3), JST. A portion of this work was carried out at the National High Magnetic Field Laboratory, which is supported by the National Science Foundation Cooperative Agreement No. DMR-1644779 and the State of Florida.

#### REFERENCES

- (1) Bowden, C. M.; Ciftan, M.; Robl, H. R. Optical Bistability; Springer Science & Business Media: Boston, MA, 2012.
- (2) Gibbs, H. Optical Bistability: Controlling Light with Light; Elsevier: Orlando, FL, 2012.
- (3) Loth, S.; Baumann, S.; Lutz, C. P.; Eigler, D. M.; Heinrich, A. J. Bistability in Atomic-Scale Antiferromagnets. *Science* **2012**, 335 (6065), 196–199.
- (4) Signorello, G.; Lörtscher, E.; Khomyakov, P. A.; Karg, S.; Dheeraj, D. L.; Gotsmann, B.; Weman, H.; Riel, H. Inducing a direct-to-pseudodirect bandgap transition in wurtzite GaAs nanowires with uniaxial stress. *Nature Commun.* **2014**, *5* (1), 3655.
- (5) Carvalho, B. R.; Wang, Y.; Mignuzzi, S.; Roy, D.; Terrones, M.; Fantini, C.; Crespi, V. H.; Malard, L. M.; Pimenta, M. A. Intervalley scattering by acoustic phonons in two-dimensional MoS<sub>2</sub> revealed by double-resonance Raman spectroscopy. *Nature Commun.* **2017**, 8 (1), 14670.
- (6) Ramasubramaniam, A.; Naveh, D.; Towe, E. Tunable band gaps in bilayer transition-metal dichalcogenides. *Phys. Rev. B* **2011**, *84* (20), 205325.
- (7) Wu, S.; Ross, J. S.; Liu, G.-B.; Aivazian, G.; Jones, A.; Fei, Z.; Zhu, W.; Xiao, D.; Yao, W.; Cobden, D.; Xu, X. Electrical tuning of valley magnetic moment through symmetry control in bilayer MoS<sub>2</sub>. *Nat. Phys.* **2013**, *9* (3), 149–153.
- (8) Wang, G.; Marie, X.; Bouet, L.; Vidal, M.; Balocchi, A.; Amand, T.; Lagarde, D.; Urbaszek, B. Exciton dynamics in WSe<sub>2</sub> bilayers. *Appl. Phys. Lett.* **2014**, *105* (18), 182105.
- (9) Jones, A. M.; Yu, H.; Ross, J. S.; Klement, P.; Ghimire, N. J.; Yan, J.; Mandrus, D. G.; Yao, W.; Xu, X. Spin-layer locking effects in optical orientation of exciton spin in bilayer WSe<sub>2</sub>. *Nat. Phys.* **2014**, *10* (2), 130–134.
- (10) Debbichi, L.; Eriksson, O.; Lebègue, S. Electronic structure of two-dimensional transition metal dichalcogenide bilayers from ab initio theory. *Phys. Rev. B* **2014**, *89* (20), 205311.
- (11) Liu, G.-B.; Xiao, D.; Yao, Y.; Xu, X.; Yao, W. Electronic structures and theoretical modelling of two-dimensional group-VIB transition metal dichalcogenides. *Chem. Soc. Rev.* **2015**, *44* (9), 2643–2663.
- (12) Lindlau, J.; Selig, M.; Neumann, A.; Colombier, L.; Förste, J.; Funk, V.; Förg, M.; Kim, J.; Berghäuser, G.; Taniguchi, T.; et al. The role of momentum-dark excitons in the elementary optical response of bilayer WSe<sub>2</sub>. *Nature Commun.* **2018**, 9 (1), 2586.
- (13) Wang, Z.; Chiu, Y.-H.; Honz, K.; Mak, K. F.; Shan, J. Electrical Tuning of Interlayer Exciton Gases in WSe<sub>2</sub> Bilayers. *Nano Lett.* **2018**, 18 (1), 137–143.
- (14) Sun, Z.; Beaumariage, J.; Cao, Q.; Watanabe, K.; Taniguchi, T.; Hunt, B. M.; Snoke, D. Observation of the Interlayer Exciton Gases in WSe<sub>2</sub> -p:WSe<sub>2</sub> Heterostructures. *ACS Photonics* **2020**, *7* (7), 1622–1627.
- (15) Förste, J.; Tepliakov, N. V.; Kruchinin, S. Y.; Lindlau, J.; Funk, V.; Förg, M.; Watanabe, K.; Taniguchi, T.; Baimuratov, A. S.; Högele, A. Exciton g-factors in monolayer and bilayer WSe<sub>2</sub> from experiment and theory. *Nature Commun.* **2020**, *11* (1), 4539.

- (16) Liu, Q.; Li, L.; Li, Y.; Gao, Z.; Chen, Z.; Lu, J. Tuning Electronic Structure of Bilayer MoS<sub>2</sub> by Vertical Electric Field: A First-Principles Investigation. *J. Phys. Chem. C* **2012**, *116* (40), 21556–21562.
- (17) Lu, X.; Yang, L. Stark effect of doped two-dimensional transition metal dichalcogenides. *Appl. Phys. Lett.* **2017**, *111* (19), 193104.
- (18) Nguyen, C. V.; Hieu, N. N.; Ilyasov, V. V. Band Gap Modulation of Bilayer MoS<sub>2</sub> Under Strain Engineering and Electric Field: A Density Functional Theory. *J. Electron. Mater.* **2016**, 45 (8), 4038–4043
- (19) Zibouche, N.; Philipsen, P.; Kuc, A.; Heine, T. Transition-metal dichalcogenide bilayers: Switching materials for spintronic and valleytronic applications. *Phys. Rev. B* **2014**, *90* (12), 125440.
- (20) Zhang, Z. Y.; Si, M. S.; Wang, Y. H.; Gao, X. P.; Sung, D.; Hong, S.; He, J. Indirect-direct band gap transition through electric tuning in bilayer MoS<sub>2</sub>. *J. Chem. Phys.* **2014**, *140* (17), 174707.
- (21) Zeng, C.; Zhong, J.; Wang, Y.-P.; Yu, J.; Cao, L.; Zhao, Z.; Ding, J.; Cong, C.; Yue, X.; Liu, Z.; Liu, Y. Observation of split defect-bound excitons in twisted WSe<sub>2</sub>/WSe<sub>2</sub> homostructure. *Appl. Phys. Lett.* **2020**, *117* (15), 153103.
- (22) Scuri, G.; Andersen, T. I.; Zhou, Y.; Wild, D. S.; Sung, J.; Gelly, R. J.; Bérubé, D.; Heo, H.; Shao, L.; Joe, A. Y.; et al. Electrically Tunable Valley Dynamics in Twisted WSe<sub>2</sub>/WSe<sub>2</sub> Bilayers. *Phys. Rev. Lett.* **2020**, *124* (21), 217403.
- (23) Sung, J.; Zhou, Y.; Scuri, G.; Zólyomi, V.; Andersen, T. I.; Yoo, H.; Wild, D. S.; Joe, A. Y.; Gelly, R. J.; Heo, H.; Magorrian, S. J.; Bérubé, D.; Valdivia, A. M. M.; Taniguchi, T.; Watanabe, K.; Lukin, M. D.; Kim, P.; Fal'ko, V. I.; Park, H. Broken mirror symmetry in excitonic response of reconstructed domains in twisted MoSe<sub>2</sub>/MoSe<sub>2</sub> bilayers. *Nat. Nanotechnol.* **2020**, *15* (9), 750–754.
- (24) Movva, H. C. P.; Lovorn, T.; Fallahazad, B.; Larentis, S.; Kim, K.; Taniguchi, T.; Watanabe, K.; Banerjee, S. K.; MacDonald, A. H.; Tutuc, E. Tunable  $\Gamma$ –K Valley Populations in Hole-Doped Trilayer WSe<sub>2</sub>. *Phys. Rev. Lett.* **2018**, *120* (10), 107703.
- (25) Liu, E.; van Baren, J.; Taniguchi, T.; Watanabe, K.; Chang, Y.-C.; Lui, C. H. Valley-selective chiral phonon replicas of dark excitons and trions in monolayer WSe<sub>2</sub>. *Phys. Rev. Research* **2019**, *1* (3), 032007.
- (26) Li, Z.; Wang, T.; Jin, C.; Lu, Z.; Lian, Z.; Meng, Y.; Blei, M.; Gao, S.; Taniguchi, T.; Watanabe, K.; et al. Emerging photoluminescence from the dark-exciton phonon replica in monolayer WSe<sub>2</sub>. *Nature Commun.* **2019**, *10* (1), 2469.
- (27) He, M.; Rivera, P.; Van Tuan, D.; Wilson, N. P.; Yang, M.; Taniguchi, T.; Watanabe, K.; Yan, J.; Mandrus, D. G.; Yu, H.; et al. Valley phonons and exciton complexes in a monolayer semiconductor. *Nature Commun.* **2020**, *11* (1), 618.
- (28) Liu, E.; van Baren, J.; Liang, C.-T.; Taniguchi, T.; Watanabe, K.; Gabor, N. M.; Chang, Y.-C.; Lui, C. H. Multipath optical recombination of intervalley dark excitons and trions in monolayer WSe<sub>2</sub>. *Phys. Rev. Lett.* **2020**, *124* (19), 196802.
- (29) Li, Z.; Wang, T.; Jin, C.; Lu, Z.; Lian, Z.; Meng, Y.; Blei, M.; Gao, M.; Taniguchi, T.; Watanabe, K.; Ren, T.; Cao, T.; Tongay, S.; Smirnov, D.; Zhang, L.; Shi, S.-F. Momentum-Dark intervalley exciton in monolayer tungsten diselenide brightened via chiral phonon. *ACS Nano* **2019**, *13* (12), 14107–14113.
- (30) Raja, A.; Selig, M.; Berghäuser, G.; Yu, J.; Hill, H. M.; Rigosi, A. F.; Brus, L. E.; Knorr, A.; Heinz, T. F.; Malic, E.; Chernikov, A. Enhancement of Exciton—Phonon Scattering from Monolayer to Bilayer WS<sub>2</sub>. *Nano Lett.* **2018**, *18* (10), 6135—6143.
- (31) Gong, Z.; Liu, G.-B.; Yu, H.; Xiao, D.; Cui, X.; Xu, X.; Yao, W. Magnetoelectric effects and valley-controlled spin quantum gates in transition metal dichalcogenide bilayers. *Nature Commun.* **2013**, *4* (1), 2053
- (32) Klein, J.; Wierzbowski, J.; Regler, A.; Becker, J.; Heimbach, F.; Müller, K.; Kaniber, M.; Finley, J. J. Stark Effect Spectroscopy of Mono- and Few-Layer MoS<sub>2</sub>. *Nano Lett.* **2016**, *16* (3), 1554–1559.

**Nano Letters** pubs.acs.org/NanoLett Letter

- (33) Lee, J.; Mak, K. F.; Shan, J. Electrical control of the valley Hall effect in bilayer MoS<sub>2</sub> transistors. Nat. Nanotechnol. 2016, 11 (5),
- (34) Das, S.; Gupta, G.; Majumdar, K. Layer degree of freedom for excitons in transition metal dichalcogenides. Phys. Rev. B 2019, 99 (16), 165411.
- (35) Arora, A.; Nayak, P. K.; Dixit, T.; Ganapathi, K. L.; Krishnan, A.; Rao, M. S. R. Stacking angle dependent multiple excitonic resonances in bilayer tungsten diselenide. Nanophotonics 2020, 9 (12), 3881-3887.
- (36) Das, S.; Dandu, M.; Gupta, G.; Murali, K.; Abraham, N.; Kallatt, S.; Watanabe, K.; Taniguchi, T.; Majumdar, K. Highly Tunable Layered Exciton in Bilayer WS2: Linear Quantum Confined Stark Effect versus Electrostatic Doping. ACS Photonics 2020, 7 (12), 3386 - 3393.
- (37) Leisgang, N.; Shree, S.; Paradisanos, I.; Sponfeldner, L.; Robert, C.; Lagarde, D.; Balocchi, A.; Watanabe, K.; Taniguchi, T.; Marie, X.; Warburton, R. J.; Gerber, I. C.; Urbaszek, B. Giant Stark splitting of an exciton in bilayer MoS<sub>2</sub>. Nat. Nanotechnol. 2020, 15 (11), 901-
- (38) Zhao, W.; Ghorannevis, Z.; Chu, L.; Toh, M.; Kloc, C.; Tan, P.-H.; Eda, G. Evolution of Electronic Structure in Atomically Thin Sheets of WS<sub>2</sub> and WSe<sub>2</sub>. ACS Nano 2013, 7 (1), 791-797.
- (39) Nguyen, P. V.; Teutsch, N. C.; Wilson, N. P.; Kahn, J.; Xia, X.; Graham, A. J.; Kandyba, V.; Giampietri, A.; Barinov, A.; Constantinescu, G. C.; Yeung, N.; Hine, N. D. M.; Xu, X.; Cobden, D. H.; Wilson, N. R. Visualizing electrostatic gating effects in twodimensional heterostructures. Nature 2019, 572 (7768), 220-223.
- (40) Kormanyos, A.; Burkard, G.; Gmitra, M.; Fabian, J.; Zolyomi, V.; Drummond, N. D; Fal'ko, V. k · p theory for two-dimensional transition metal dichalcogenide semiconductors. 2D Mater. 2015, 2 (2), 022001.
- (41) Huang, Z.; Zhao, Y.; Bo, T.; Chu, Y.; Tian, J.; Liu, L.; Yuan, Y.; Wu, F.; Zhao, J.; Xian, L. Spatially indirect intervalley excitons in bilayer WSe2. Phys. Rev. B 2022, 105, L041409.

# **□** Recommended by ACS

# Dynamic Tuning of Moiré Excitons in a WSe<sub>2</sub>/WS<sub>2</sub> Heterostructure via Mechanical Deformation

Wenyu Zhao, Feng Wang, et al.

OCTORER 18 2021

NANO I FTTERS

READ 2

Quantum Nature of THz Conductivity: Excitons, Charges, and Trions in 2D Semiconductor Nanoplatelets and Implications for THz Imaging and Solar Hydrog...

Michael T. Quick, Alexander W. Achtstein, et al.

JUNE 09, 2022

ACS APPLIED NANO MATERIALS

READ **C** 

# **Excitonic Energy Transfer in Heterostructures of Quasi-**2D Perovskite and Monolayer WS2

Qi Zhang, Goki Eda, et al.

AUGUST 07, 2020

ACS NANO

READ **C** 

# Interlayer Exciton Transport in MoSe<sub>2</sub>/WSe<sub>2</sub> Heterostructures

Zidong Li, Parag B. Deotare, et al.

JANUARY 08, 2021

ACS NANO

READ **C** 

Get More Suggestions >